Tropical Cyclone Formation in a Sheared Environment: A Case Study

JOHN MOLINARI, DAVID VOLLARO, AND KRISTEN L. CORBOSIERO

Department of Earth and Atmospheric Sciences, University at Albany, State University of New York, Albany, New York

(Manuscript received 23 June 2003, in final form 25 May 2004)

ABSTRACT

The development of Hurricane Danny (1997) from depression to hurricane was examined using cloud-to-ground lightning data, reconnaissance aircraft data, and satellite imagery. Vertical wind shear between 850 and 200 hPa of 5–11 m s^{-1} produced persistent downshear convective outbreaks that became progressively more intense and closer to the center during the development. Early in the period the storm intensified steadily in the presence of this downshear convection. During the last and most intense outbreak, a second vortex appeared to develop within the convection. Evidence is presented that the new downshear vortex became the dominant vortex and absorbed the original. Based on these events, it is hypothesized that the presence of moderate vertical wind shear accelerated the early development process.

Equivalent potential temperature fields within 500 m of the surface were examined. Only well after the period of vortex interaction did the characteristic mature tropical cyclone radial profile of equivalent potential temperature appear. This came about by the virtual elimination of both low θ_e values in the core and high θ_e values outside the core that had been present at previous hours.

The growth of Hurricane Danny is viewed in terms of the wind-induced surface heat exchange (WISHE) theory. During the tropical depression and early tropical storm (''pre-WISHE'') periods, few if any of the assumptions of WISHE were met: vertical wind shear exceeded 5 m s^{-1}, considerable azimuthal asymmetry was present, transient highly buoyant convection occurred, and low values of θ_e in the storm core suggested the presence of convective downdrafts. It is proposed that 1) vortex interactions and subsequent axisymmetrization produced a single dominant vortex at the surface, and 2) vertical mixing of moist entropy by strong convection moved the sounding toward moist neutrality. By this reasoning, the disturbance then met the key tenets of the known finite-amplitude WISHE instability, and the storm intensified to hurricane strength.

1. Introduction

Pasch (1998) described the history of Hurricane Danny (1997). A series of mesoscale convective systems (MCSs) occurred over the lower Mississippi River valley and the northern Gulf of Mexico on 13–14 July 1997. Surface pressure decreased over the north-central Gulf of Mexico, and a weak cyclonic circulation developed at the surface on 15 July. Little organized convective activity occurred until near 1200 UTC 16 July. The first advisory was issued at 2038 UTC on 16 July after the first aircraft reconnaissance flight, but the depression formation was retroactively set 8 h earlier to 1200 UTC. At that time, maximum surface winds were estimated to be 25 kt. Development was slow until about 1200 UTC 17 July, when the intensity and areal coverage of deep convection increased dramatically. A reconnaissance flight near 1500 UTC the same day reported tropical storm force winds, and the system was declared a tropical storm retroactively to 1200 UTC 17 July. Intensification continued to hurricane strength by 0600 UTC 18 July. Hurricane Danny weakened slightly as it crossed a narrow part of the southeastern tip of Louisiana, but maintained hurricane strength until after its landfall in Alabama near 1700 UTC 19 July. The storm produced intense rainfall (up to 100 cm) during and after landfall (Blackwell 2000).

Figures 1a,b show two tracks for Hurricane Danny. The first (Fig. 1a) gives real-time positions for each storm advisory put out by the Tropical Prediction Center (TPC), while the second gives 6-hourly positions from the best-track locations determined after the season. TPC advisories are normally issued every 6 h near 0300, 0900, 1500, and 2100 UTC. Advisories 1–4 and 6–7 followed this schedule. Two additional advisories are shown in Fig. 1a: a special advisory (No. 5 in the figure) and an intermediate advisory (No. 5a) 2 h later. The real-time advisories show a nearly stationary storm on 16 July and early 17 July. The storm then moved north-northeastward at 2–3 m s^{-1} through 1440 UTC 17 July. At 1545 UTC, the special advisory indicated that a new center had formed 120 km to the northeast. The storm then meandered for several hours before renewing its northeastward motion. This erratic behavior reported in

Corresponding author address: J. Molinari, Dept. of Earth and Atmospheric Sciences, University at Albany, State University of New York, Albany, NY 12222.
E-mail: molinari@atmos.albany.edu

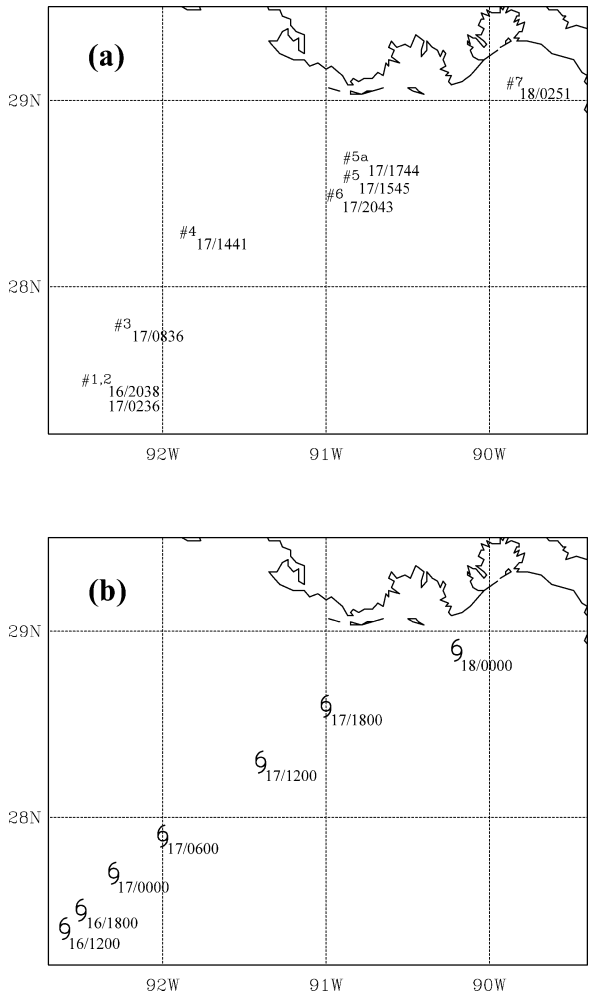

FIG. 1. (a) Positions of depression/Tropical Storm/Hurricane Danny for each of the first seven advisories issued by the TPC in real time, plus the same for an intermediate advisory (No. 5a) when a new center formed. The exact positions lie at the lower left corners of the No. symbols. The day and time is shown at the lower right of each advisory position. (b) Six-hourly best-track positions.

real time was smoothed in the best track, but it will be argued in this paper that the real-time positions give some insight into the structure and dynamics of the multiple centers within the developing cyclone.

In summary, Hurricane Danny in its early stages exhibited complex behavior. Both depression and tropical storm declarations were made retroactively after aircraft reconnaissance showed additional strengthening, and the center of the storm was difficult to track and appeared to reform at a new position.

During the entire period from predepression to hurricane stage, the center of the disturbance that was to become Hurricane Danny remained within range of the ground-based National Lightning Detection Network (NLDN). In this paper cloud-to-ground lightning data, as well as satellite images and aircraft reconnaissance data, will be utilized to address the following questions concerning the genesis of Hurricane Danny. 1) Why did the center reform? 2) How was intensification to tropical storm strength able to occur so quickly at the new center location? 3) What was the role of vertical wind shear? 4) How can the sequence of events be interpreted in terms of current hypotheses on the genesis of tropical cyclones?

2. Data sources

Lightning data were obtained from archived observations of the NLDN, which is described by Orville (1991). The current configuration of the NLDN, which was upgraded in 1994, is given by Cummins et al. (1995). The greater sensitivity and accuracy of the upgraded network has been confirmed by Idone et al. (1998a,b). Within the network over land the detection efficiency of stronger flashes (greater than 14-kA peak current) was nearly 100%. Median location errors in the vicinity of Albany, New York, were less than 1 km (Idone et al. 1998b). No ground truth is available over water, but Molinari et al. (1994, 1999), Samsury and Orville (1994), and Corbosiero and Molinari (2002, 2003) have shown that the location accuracy and the detection efficiency of the NLDN in the region within about 400 km of the United States coastline are sufficient to describe the convective structure of tropical cyclones. A great benefit of the NLDN is its continuous coverage of ground flashes in space and time within range of the network.

Broad inferences will be made about vertical velocity based on cloud-to-ground lightning frequency. Baker et al. (1999), in a numerical study of convection with electrification included, found that total lightning flash rate (ground flashes plus intracloud flashes) is proportional to the fourth power of the local upward vertical velocity. It is likely that the ground flash rate alone, which is measured by the NLDN, is also a sensitive measure of vertical velocity. Baker et al.'s results imply that lightning frequency should increase dramatically with vertical velocity, and a lack of lightning should indicate relatively small vertical velocities. Zipser and Lutz (1994) argued that the rapid electrification needed for lightning flashes requires mean updrafts of 6–7 m s^{-1} over the layer between the melting level and the -20°C level (roughly 4.5–8.0 km). Cecil and Zipser (2002) showed that lightning is accompanied by large reflectivity reaching well above the melting level. Both Zipser and Lutz (1994) and Black and Hallett (1999) noted that localized updrafts of greater than 10 m s^{-1} were required to create charge separation sufficient to produce lightning. The mean upward motion over a *mesoscale* region of lightning (order of 50 km in diameter) would likely be less than 10 m s^{-1}. In this paper, it will be shown that a 1–2 m s^{-1} mean updraft at $z = 6$ km within a mesoscale region of intense lightning would be sufficient to produce substantial vortex spinup. Based on the literature above, the assumption of such an updraft in

TABLE 1. Times of U.S. Air Force reconnaissance flights during the period of interest. One flight in which data were unreliable is not listed. All times the aircraft was in the air are included, not just the times in the storm.

Aircraft	Starting time	Ending time
AF980	1651 UTC 16 Jul	1902 UTC 16 Jul
AF967	1726 UTC 16 Jul	2317 UTC 16 Jul
AF980	1348 UTC 17 Jul	2010 UTC 17 Jul
AF966	2214 UTC 17 Jul	0836 UTC 18 Jul
AF963	1052 UTC 18 Jul	2106 UTC 18 Jul
AF963	0355 UTC 19 Jul	0909 UTC 19 Jul

the presence of frequent cloud-to-ground lightning does not seem unwarranted.

In subsequent sections of the paper, 6-hourly best-track positions, interpolated to hourly, will be used to define the storm center in order to gauge the storm-relative variability of a number of quantities. As noted earlier (Fig. 1), real-time positions give some evidence for center reformation and the simultaneous presence of two centers. The best-track center can be viewed as a centroid of multiple centers when they are present. Such an estimate is more stable for tracking the time variation of quantities. The most accurate center positions existed when U.S. Air Force reconnaissance aircraft were in the storm. Table 1 gives the start and end times for all the flights into Danny during the period of interest in this paper. One flight beginning about 2100 UTC 18 July contained questionable data due to instrument problems and is not listed. During the flight times given in Table 1, the interpolated best-track center positions followed the real-time reconnaissance estimates closely. Unfortunately, no flights were made between 0000 UTC and 1345 UTC 17 July, and storm-relative distributions must be considered questionable during this time. This limitation will be addressed as the results are presented.

Equivalent potential temperature (θ_e) will be calculated following Bolton (1980) from temperature and moisture values collected by U.S. Air Force reconnaissance flights. One potential source of measurement error can arise due to wetting of the temperature sensor, which leads subsequently to evaporative cooling and a spuriously low temperature reading, and thus a low θ_e estimate. Eastin et al. (2002) found that 90% of such errors occurred within cloud. The air force reconnaissance data of interest in this study was collected between the 200- and 500-m levels above the ocean, where cloud is much less likely than aloft, and sensor wetting errors should be minimized. Nevertheless, Eastin et al. (2002) note that in the absence of cloud, precipitation can also produce wetting problems. The existence of even small regions with such temperature errors makes quantitative analysis of the distribution of θ_e difficult. The high values are likely to be accurate, but the low values might sometimes be accurate (owing to cold downdrafts, for instance) and sometimes be inaccurate due to sensor wetting. As a result, the θ_e values will be shown as scatterplots versus radius in the fashion of Raymond et al. (1998). Emphasis will be on the general patterns, with focus on the high-value end of the distribution. It will be shown that despite the uncertainties, considerable information is present in these data.

TABLE 2. Vertical wind shear in Hurricane Danny averaged over 500 km of radius for the period of interest in this study. Danny was named a tropical storm at 1200 UTC 17 Jul, and a hurricane at 0600 UTC 18 Jul.

Date/time (UTC)	Direction (deg)	Magnitude (m s^{-1})
16 Jul 1200	325	8.4
1800	300	4.9
17 Jul 0000	263	7.3
0600	299	10.6
1200	320	9.3
1800	310	6.1
18 Jul 0000	272	8.2
0600	288	11.5
1200	297	8.8
1800	251	2.7
19 Jul 0000	231	3.0
0600	267	5.8
1200	175	1.3

Aircraft reconnaissance estimates of the radius of maximum winds (RMW) will also be described in this study. Typically four to six estimates make up the value used for any given flight, and all four quadrants are sampled. At the early stages of a storm, the RMW estimates are only approximate and often differ significantly from quadrant to quadrant. At best, they should be taken as accurate within 10–15 km during tropical depression stage, and become progressively more accurate as the storm intensifies.

Vertical wind shear is calculated from European Centre for Medium-Range Weather Forecasts (ECMWF) analyses between the 850- and 200-hPa levels over a 500-km radius from the storm center. As noted by Molinari et al. (1995), the ECMWF analyses are particularly reliable for studying the environment of hurricanes within a few hundred kilometers of the United States rawinsonde network. Because mean Cartesian wind components are calculated on a cylindrical grid at the two levels, the method removes the axisymmetric part of the vertical shear (which is representative of the change with height of the mean vortex itself) and determines cross-storm shear only (Hanley et al. 2001). Corbosiero and Molinari (2002) provide evidence that calculated shears are likely to be within 1–2 m s^{-1} of the true vertical wind shear averaged over 500 km.

3. Environmental conditions during the life cycle of the storm

Table 2 gives the 850–200-hPa vertical wind shear direction and magnitude in 6-hourly increments starting from the depression stage of Danny and ending just before landfall. Wind shear was from the west or northwest throughout the prehurricane period, and ranged in magnitude from 5–11 m s^{-1}. It is notable that vertical

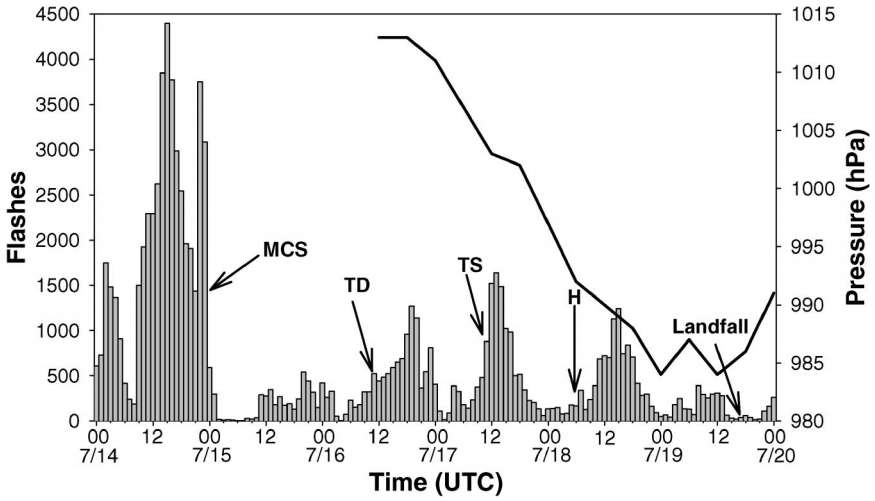

FIG. 2. Evolution of the number of ground flashes in a region 5° lat × 6° lon centered on the storm. For times before depression formation at 1200 UTC 16 Jul 1997, the region is centered on the location of depression formation. The solid line gives the best-track minimum central pressure, available from the time of depression formation.

wind shear did not fall below 5 m s^{-1} until 1800 UTC 18 July, 12 h *after* hurricane intensity was reached. Danny intensified from depression to storm (as determined by the Tropical Prediction Center) in the presence of vertical shear of 9 m s^{-1}, and from storm to hurricane in shear of greater than 11 m s^{-1}. It will be shown in later sections that convective outbreaks occurred persistently downshear of the center throughout the development period, consistent with the findings of Corbosiero and Molinari (2002).

Sea surface temperatures (averaged from 7 to 13 July, before the storm formed, not shown) varied only from 29.8° to 29.9°C along the path of Danny between depression and initial hurricane strength. This suggests favorable sea surface forcing with almost no change along the track. Sea surface heights from Ocean Topography Experiment (TOPEX) and *European Remote Sensing Satellite–2* (*ERS-2*) instruments (also not shown) contained values close to climatology throughout the period, with height anomalies less than 10 cm along the track through the time hurricane strength was reached. Thus, although surface temperatures before cyclogenesis were high, the ocean mixed layer heat content seemed to be about average for the time of year. Finally, the climatological sea surface height also varies by less than 10 cm along the track of Danny. Because so little variation in ocean properties occurred along the track during the formation process, these variables will not be considered further when diagnosing the evolution of Danny, except to note that ocean conditions should not have inhibited development.

Bracken and Bosart (2000) have noted that interactions with upper troughs can be critical during formative stages (see also Montgomery and Farrell 1993; Bosart and Bartlo 1991; Davis and Bosart 2001). Molinari and Vollaro (1989) measured such interactions using eddy flux convergence of angular momentum. DeMaria et al. (1993) used an upper tropospheric spinup by this process of 10 m s^{-1} day^{-1} as a threshold for significant events, and Hanley et al. (2001) required in their definition of a trough interaction that the same threshold be met between the 300–600-km radii for at least two consecutive 12-h periods. Using either of these criteria (figure not shown), no trough interaction occurred during the formation of Hurricane Danny, and this factor will also be eliminated from consideration.

4. Overview of lightning evolution during the development of Hurricane Danny

Figure 2 shows the number of flashes occurring in a region 5° latitude × 6° longitude centered on the moving storm. For times prior to depression formation at 1200 UTC 16 July, for which no center position was available, the box was centered on the location of depression formation. Because the system was nearly stationary for more than 48 h before depression formation (Pasch 1998), this procedure should be satisfactory. After 1200 UTC 16 July, the best-track center positions are used. The pressure trace from the best-track data is also shown in Fig. 2 from the time of depression development onward.

Large flash rates (frequently exceeding 2000 h^{-1}) occurred on 14 July, the first day shown on Fig. 2. These are typical of an MCS regime (MacGorman and Rust 1998, their Fig. 8.39). After 14 July, however, Fig. 2 shows that lightning over the broad area surrounding the predepression disturbance became and remained less frequent right through to the landfall of Hurricane Danny. Flash rates much smaller than in MCSs are characteristic of tropical cyclones in general (Molinari et al. 1999). Three major outbreaks of lightning occurred on

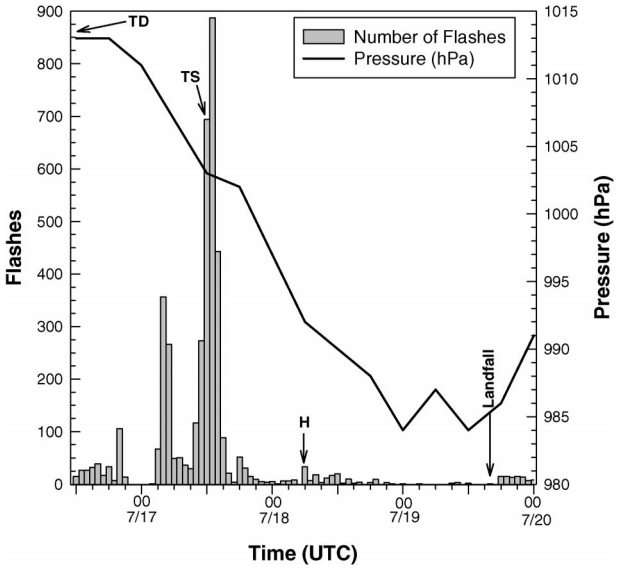

FIG. 3. Time series of the number of flashes within 100 km of the center of Hurricane Danny (histogram), beginning with formation of the depression on 1200 UTC 16 Jul. Also shown (solid line) is the minimum central pressure.

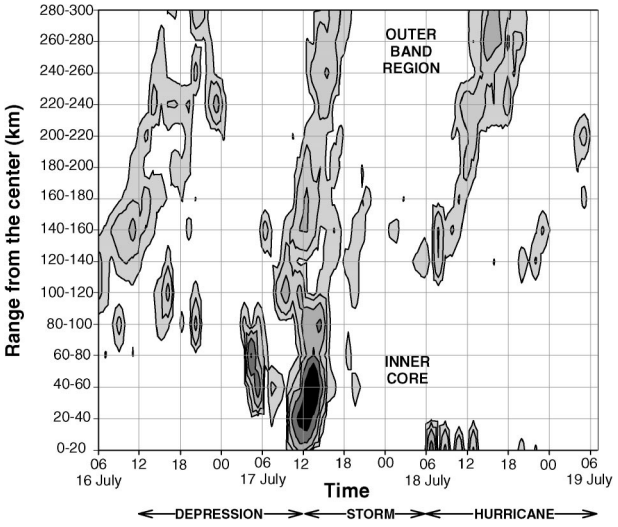

FIG. 4. Radius–time series of hourly ground flash density in each 20-km radial bin. Contours are in powers of 2: 20, 40, 80, 160, 320, 640 flashes (100 km)$^{-2}$ h^{-1}. Light shading is 20–79 flashes (100 km)$^{-2}$ h^{-1}; medium shading is 80–159 flashes (100 km)$^{-2}$ h^{-1}; dark gray is 160–319 flashes (100 km)$^{-2}$ h^{-1}; and black shading is $>$320 flashes (100 km)$^{-2}$ h^{-1}.

this large scale surrounding Danny, centered on 1800 UTC 16 July, 1300 UTC 17 July, and 1500 UTC 18 July. A modest indication of a diurnal cycle in convection is present, with the above maxima occurring between 0700 and 1200 LT, and minima occurring within 3 h of 0000 UTC (early evening local time).

Lightning activity of greatest significance to tropical cyclone intensity change occurs close to the core (Molinari et al. 1999). Figure 3 shows a time series of ground flashes within 100 km of the storm center, starting from the beginning of tropical depression stage at 1200 UTC 16 July. Lightning developed in this region during 16 July, peaking in the hour centered on 1700 UTC when more than 100 flashes occurred. A second more intense outbreak of about 300 flashes per hour took place from 0400–0500 UTC 17 July. The most powerful outbreak of lightning occurred from 1000–1400 UTC the same day, reaching almost 900 flashes per hour. This hourly frequency exceeded that of any outbreak within 100 km of the center of any tropical cyclone over water within range of the NLDN over the period 1985–2001. Danny was declared a tropical storm retroactively to the time of this last outbreak.

Relatively little lightning occurred during the following 48 h leading up to landfall in Alabama. This relative lack of lightning in the inner core, even as minimum central pressure continued to fall, is not uncommon (Molinari et al. 1994, 1999). It likely represents a shift from strongly buoyant deep convection to the less buoyant 1–4 m s^{-1} updrafts that are most common in the hurricane core in the lower-troposphere (Black et al. 1996), and generally less than 10 m s^{-1} updrafts aloft (Marks and Houze 1987), too weak for significant lightning generation.

Figure 4 shows a radius–time section of hourly lightning flash density in 20-km radial bins. Flash density is chosen rather than flash frequency in order to normalize by the area of each annular ring. It is expressed as the number of ground flashes per 10 000 km^2 (i.e., 100 km $\times$ 100 km box) per hour. Figure 4 shows that the diurnal variation noted in Fig. 2 occurred primarily in the outer bands. For 3 consecutive days, lightning developed near the 140-km radius at about 1200 UTC. The flash density maximum shifted outward with time at a speed of 5–10 m s^{-1}. This distinct phenomenon no longer occurred after landfall (not shown).

Of greater significance to the tropical cyclone formation process is the radial distribution of lightning in the storm core shown in Fig. 4. A maximum appeared in the 100–120-km radial region on 16 July at 1600 UTC, and a second maximum at the 80–100-km radius occurred at 2000 UTC on the same day (the first of these does not show in Fig. 3, which covered only the inner 100 km). A much more intense outbreak occurred at 0400–0500 UTC 17 July at the 60–80-km radius, and the final very intense outbreak was centered at 1200–1300 UTC the same day in the 40–60-km radial range. After this major outbreak, little lightning occurred in the storm core for more than 12 h, followed by only localized maxima at the innermost 20 km of radius during the first few hours at hurricane intensity.

Figure 5 shows the radial distribution of average flash density for two extended periods: the prehurricane period from 1200 UTC 16 July to 0559 UTC 18 July, and the time of hurricane strength from 0600 UTC 18 July

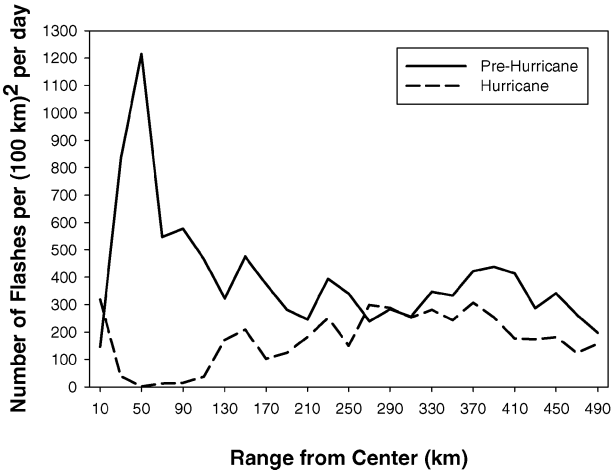

FIG. 5. Radial distribution of ground flash density per day [units: flashes (100 km)$^{-2}$ day^{-1}] within 20-km bins. Solid line is averaged over the prehurricane stage of Hurricane Danny (1200 UTC 16 Jul to 0559 UTC 18 Jul 1997). Dashed line is averaged over the hurricane stage (0600 UTC 18 Jul to 0000 UTC 20 Jul 1997).

to 0000 UTC 20 July, just after landfall. In Fig. 5, flash density is given as flashes per unit area per day (following Molinari et al. 1994) rather than per hour as in Fig. 4. Outside the 200-km radius, the flash density was slightly smaller during hurricane stage. Within the 200-km radius the flash density decreased more dramatically at all radii except the inner 20 km of radius. After hurricane intensity was reached, maximum flash density occurred in the innermost 20 km, and a region of strongly suppressed lightning developed between the 20- and 120-km radii.

This evolution is consistent with the radial distribution of flash density shown by Molinari et al. (1994, 1999): the radial distribution of flashes in tropical storms resembled the solid line in Fig. 5, while that in hurricanes resembled the dashed line. The characteristic hurricane lightning distribution with radius appears in Fig. 5: an eyewall maximum, a sharp minimum extending beyond the 100-km radius, and a large outer-rainband maximum that is little changed from its value during the prehurricane stages. The benefit of the current study is that the evolution has been captured in a single storm that remained within range of the NLDN throughout the formation process.

None of the previous figures gives a measure of the azimuthal distribution of lightning. Figure 6 shows an azimuth-time series of flash counts for the region within the 100-km radius. Following Corbosiero and Molinari (2002), the azimuthal distributions in Fig. 6 are shown with respect to the 6-hourly vertical wind shear vector rather than by geographical direction. The shaded region indicates the two octants that are directly downshear of the storm center at each observation time. The units are number of flashes per octant per hour. Figure 6 shows a dramatic preference for ground flashes to occur downshear of the center. Consistent with Fig. 3, which showed the sum of the numbers in Fig. 6 across all azimuths, the intensity of this downshear convection strengthened with time: the downshear maximum at 1200 UTC 17 July is 20 times more intense than any event on 16 July, and 4 times as intense at the first event at 0400–0500 UTC 17 July. Only the final convective outbreak extended significantly beyond the downshear octants, but the maximum flash frequency still remained downshear.

In summary, the lightning data show repeated episodes of downshear convection, each one more intense and closer to the center. After the most intense such event, lightning activity dramatically lessened as the storm intensified into a hurricane. The data presented thus far do not indicate how the center might have reformed after the major lightning outbreak, and what role that reformation might have played in the subsequent intensification. These issues will be addressed in the following section.

5. Satellite and reconnaissance aircraft view of intensification

a. Clouds, lightning, and winds

As noted earlier, TPC identified a region of active MCS formation on 14 July, and a surface low-pressure area in the vicinity of the previous MCSs on 15 July. Convection occurred downshear of the disturbance on 15 July, but with relatively low intensity as measured by lightning and satellite signatures. On 16 July, more frequent downshear convection developed (Figs. 3, 6; vertical wind shear is given in Table 2). Figure 7 shows an infrared (IR) satellite image at 2200 UTC 16 July during the first reconnaissance flight into the storm. The outer edges of cyan and green shading represent 228 and 212 K, respectively. Also shown are surface observations, reconnaissance aircraft–measured winds, and locations of cloud-to-ground lightning flashes. Reconnaissance winds in Fig. 7, as well as at all other times that will be shown in this paper, were collected below the 500-m level and thus represent boundary layer winds. Figure 7 also shows contours of surface wind speed from the operational H*Wind analyses (Powell et al. 1998). These analyses include all possible real-time data sources, but in this region primarily represent the reduction of reconnaissance flight-level winds to the surface.

Figure 7 indicates that convection was highly asymmetric on 16 July, with high clouds and lightning predominantly in the downshear half of the lower-tropospheric circulation, consistent with Fig. 6. Only a few scattered high clouds appeared upshear, where shear-induced subsidence would be expected (Sutcliffe 1947; DeMaria 1996; Frank and Ritchie 2001). A closed circulation existed near the surface, with strongest winds downshear of the center. No evidence of multiple centers at flight level was present.

As indicated in Figs. 3, 5, and 6, active convection

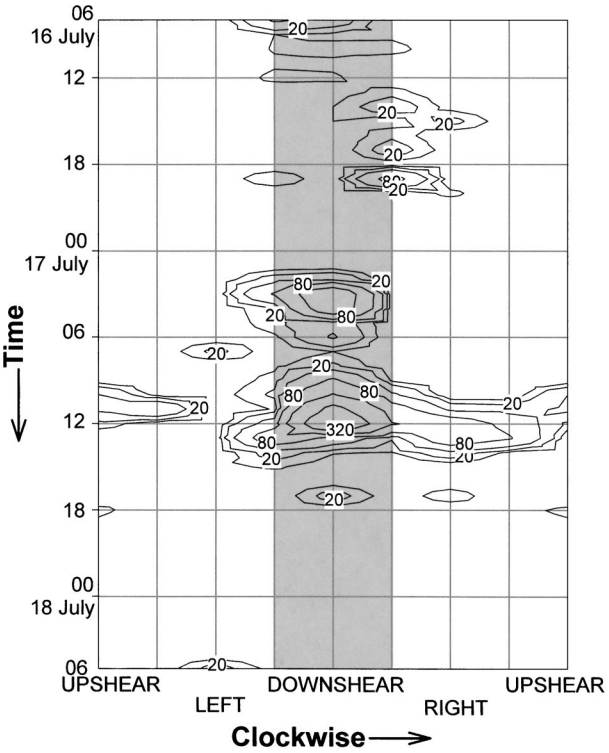

FIG. 6. Azimuth time series of the number of flashes within 100 km of the center of Hurricane Danny, counted in octants. The azimuthal locations of each flash have been rotated with respect to the vertical wind shear vector during each 6-h period, following Corbosiero and Molinari (2002). The octants are thus with respect to the shear vector; the horizontal axis represents a clockwise turning from upshear to downshear and back. Shading represents the two downshear octants. ''Right'' and ''left'' always are with respect to the vertical wind shear vector. Because few flashes occurred within 100 km of the center after 0600 UTC 18 Jul (see Fig. 3), the figure terminates at that time. Contours are in powers of 2, beginning with 10 flashes per octant per hour.

decayed during the 4 h following the time of Fig. 7. The circulation became difficult to identify in the cloud field. At 0300 UTC 17 July, a small region of lightning developed downshear and rapidly intensified over the following 2 h, as shown earlier. The number of flashes per unit area and per unit time grew to several times previous maxima in the storm. Figure 8 shows an infrared satellite image of the storm at 0845 UTC 17 July using the 3.9-μm channel of the *Geostationary Operational Environment Satellite–8* (*GOES-8*). This channel is more sensitive to low clouds than the standard 10.7-μm channel (Brown et al. 1995), but tends to pixelize high clouds. In Fig. 8, all clouds colder than 244 K are shaded a uniform dark brown. The light blue shading indicates cloud-top temperatures between 291 and 275 K, but most of the values shown lie between 291 and 283 K. This shading thus represents clouds that lie primarily below the 700-hPa level.

The time of Fig. 8 lies about halfway between the first big downshear convective outbreak at 0400–0500 UTC and the second at 1200–1300 UTC. It is apparent that the low-level circulation remained upshear of the strongest convection. The cyclonically curved band of lightning and high cloud to the north suggests that the storm circulation was strengthening. The beginning of what was to become the most intense downshear cell can be seen from the first three flashes southeast of the center near 28°N.

Figure 9 shows a standard infrared satellite image (as in Fig. 7) for 1200 UTC 17 July, near the time the downshear cell was most intense. The 3.9-μm channel has little value for identifying low clouds as soon as any visible light is present, and thus was not used at this hour. Two oil rigs (black wind barbs) reported at this time, and the center of the storm almost certainly lies between them. The oil rig observations were not taken at the standard 10-m level, but were near 100 m, well within the boundary layer. It is apparent from the observed 70-kt wind that the vortex has strengthened, even if the high wind speed partly indicates the presence of localized convective features. The system was officially named a tropical storm at this hour. The tropical storm symbol in the Fig. 9 indicates the best track center position.

The most striking aspect of Fig. 9 is the new convective outbreak just downshear of the best-track center. As noted earlier, this outbreak was not only the strongest in this storm (Figs. 3, 4, and 6), but also contained more flashes per hour within 100 km of the center over water than in any storm sampled by the NLDN over 17 yr. The evolution of this outbreak is shown using lightning locations over 2-h time increments in Fig. 10. Radius lines and the best-track center valid at 1200 UTC are shown for reference, but this figure gives true flash positions with respect to the geography. Although the best track center is uncertain during this time, there is little doubt that the lightning maximum rotated cyclonically around the original center. By the end of the period (1330–1529 UTC, in blue), the flash count dropped significantly. Shown in Fig. 10 is the location of the reformed center reported by TPC and aircraft reconnaissance at 1448 UTC. This center lies just radially inward from the remains of the downshear cell. If the original center moved to this position from its 1200 UTC position, it would imply a speed of motion of 5.0 m s^{-1}, which is greater than the mean tropospheric flow over 500 km of radius of 3.1 m s^{-1} at 1200 UTC. This difference offers some support for the TPC report of a downshear reformation rather than the original center remaining the primary circulation in the storm. Figure 10 also shows the 1915 UTC storm center position as defined by the first appearance of an eyelike feature in visible satellite imagery. The storm moved at an average speed of only 1.1 m s^{-1} between 1448 and 1915 UTC. It will be argued below that this motion, which is slower than the tropospheric mean flow of 2.6 m s^{-1} at 1800 UTC, might relate to an interaction between the reformed center and the original center.

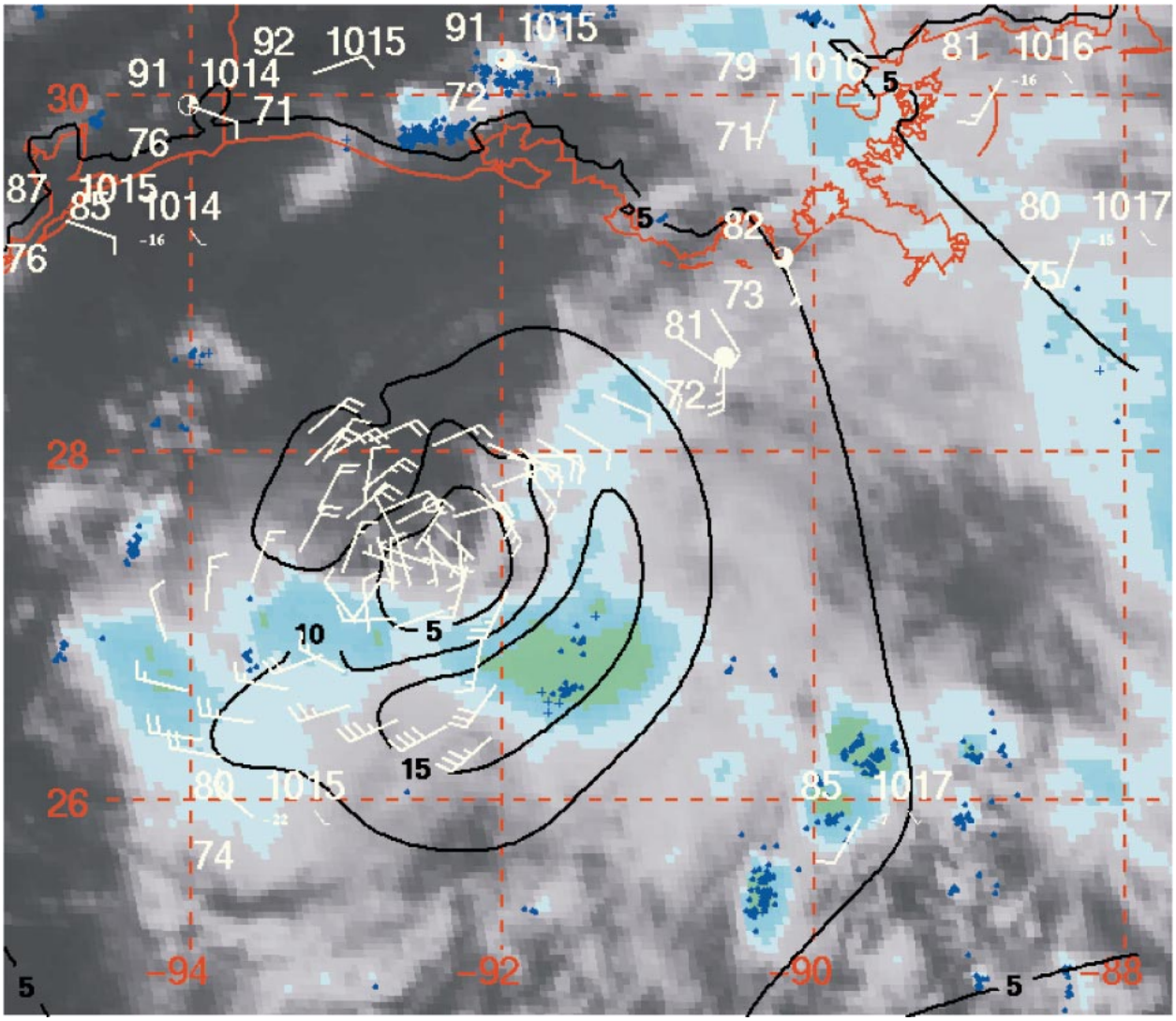

FIG. 7. Infrared satellite image for 2200 UTC 16 Jul 1997. Cyan and green shadings begin at cloud-top temperatures of 228 and 212 K, respectively. Blue dots and plus signs indicate locations of cloud-to-ground lightning flashes with negative and positive polarity, respectively. Black contours represent surface wind speed (increment 5 m s^{-1}) based on the operational H*Wind analyses (see Powell et al. 1998). Conventional surface data are shown in yellow.

Figure 11 provides a means of addressing the nature of possible vortex interactions after the hypothesized downshear spinup has occurred. The left panels show vorticity at hours 0, 6, and 12 of an idealized barotropic simulation by Enagonio and Montgomery (2001, their Fig. 12c). The right panels show infrared satellite images at 1300 UTC 17 July, 1900 UTC 17 July, and 0100 UTC 18 July. The filled red circle in the two lower right panels represents the position of the eyelike feature noted earlier. The time scale of interaction in the idealized simulation and in nature appeared similar enough to use the same hours for each. In the idealized simulation, a small, intense vortex was initially placed directly east of a larger, weaker vortex. This would be crudely representative of the situation in the top right panel, if rapid spinup were occurring within the intense downshear cell that had shifted to nearly east of the larger tropical storm circulation at 1300 UTC. The vorticity evolution in the left panels will be contrasted with the high cloud evolution on the right. Unlike the simulation, the real storm is baroclinic and contains active convection. The basis for the comparison is that once two lower-tropospheric vortices are present in nature, vorticity evolution will be dominated temporarily by their interaction, and in part convection will follow the distribution of vorticity. The remarkable correspondence between nondivergent barotropic simulations of the hurricane core and structures in real hurricanes (e.g., see Kossin and Schubert 2004) gives support for this interpretation. The storm in nature moves toward the northeast, while the ideal-

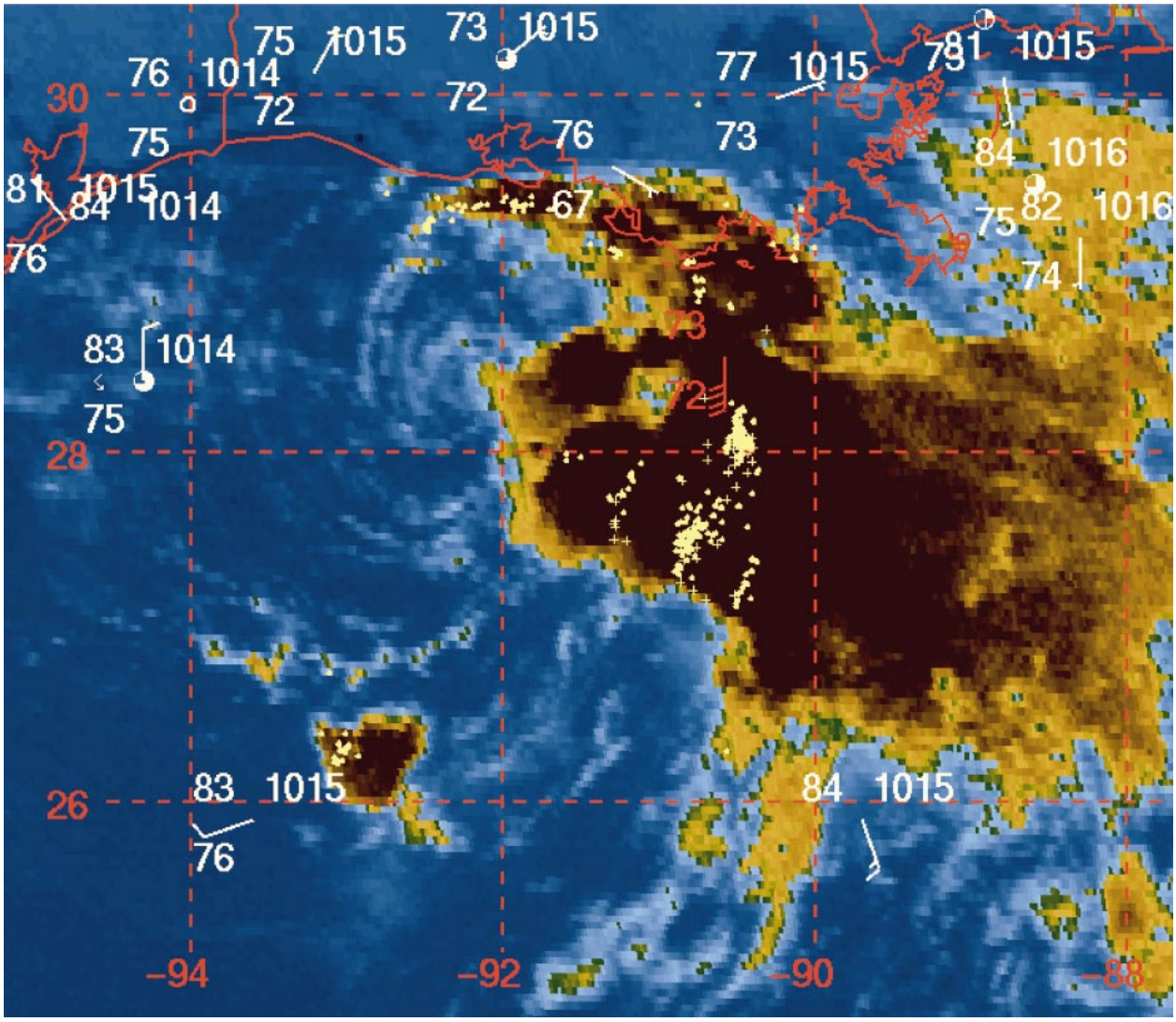

FIG. 8. Infrared satellite image at 0845 UTC 17 Jul from the 3.9-μm channel that enhances low-level cloudiness at night. Light blue shading represents cloud-top temperatures as low as 275 K, but mostly between 283 and 291 K, thus in the lower troposphere. Dark brown shading indicates temperatures below 244 K, and the medium browns represent cloud-top temperatures between these two values. Locations of cloud-to-ground lightning flashes are as in Fig. 7, except in yellow.

ized vortex in Fig. 11 does not. This simply reflects the presence of a mean flow in nature, and its absence in the simulation.

By hour 6 of the idealized simulation (middle left panel of Fig. 11), the larger vortex was deformed and wrapped cyclonically around the smaller vortex. Almost no sign of the large vortex remained directly west of the now dominant small vortex. If convection followed vorticity, the highest clouds on satellite at this hour should have been east and south of the center, with a small extension of convection southwest of the center at larger radii. This structure showed reasonably well at 1900 UTC in the cloud and lightning fields (middle right panel). By hour 12 of the idealized simulation (lower left panel), the highest vorticity outside the core was found north and east of the center, with a filament extending to south of the center. No high vorticity remained west and southwest of the center. The cloud field in the lower right satellite image showed many of the same features: high clouds north and east, a narrow maximum extending to south of the core, and absolutely no deep convection to the west or southwest.

Figure 11 gives support to the hypothesis that the downshear cell became the dominant vortex in the system. If the downshear vortex were not stronger than the original vortex, the outcome would have been much different, as shown by Enagonio and Montgomery (2001, their Fig. 12a), in which a smaller, less intense vortex was placed east of a larger, more intense vortex. In those circumstances, the evolution of vorticity looked

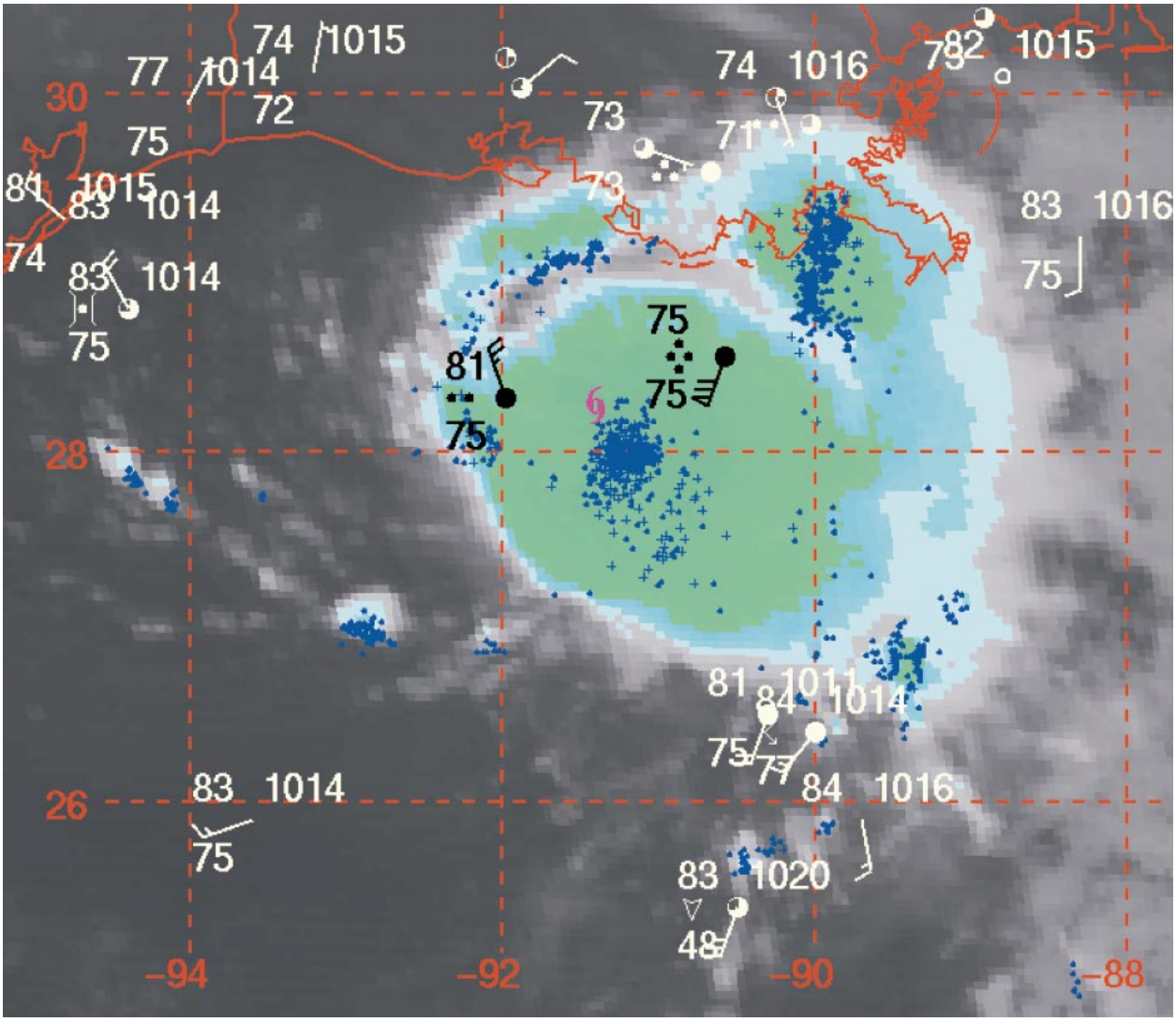

FIG. 9. As in Fig. 7, but for 1200 UTC 17 Jul 1997. In addition, the tropical storm symbol indicates the best-track center position, and data in black are from oil rigs.

nothing like Fig. 11; instead, a fairly rapid axisymmetrization occurred, and there were no filaments like that shown in the bottom panels of Fig. 11. The evolution of cloud asymmetries supports the occurrence of a rapid downshear reformation and intensification of the storm.

The small vortex in the idealized simulation was 4 times stronger (in its maximum vorticity) than the large vortex. The vorticity generation needed to create such a vortex can be estimated from the product of absolute vorticity and divergence in the downshear cell. Based on the near-surface winds shown in Fig. 9, relative vorticity in the vicinity of the downshear cell was equivalent to that of a 15–20 m s^{-1} wind at an 80-km radius, or 2–2.5 $\times$ 10^{-4} s^{-1}. Adding the Coriolis parameter gives an absolute vorticity of approximately 2.5–3 $\times$ 10^{-4} s^{-1}. Mean lower-tropospheric divergence will be obtained from mass continuity for a given midtropospheric vertical velocity. A vertical velocity of 1–2 m s^{-1} at the 6-km level gives a mean horizontal convergence between the surface and midtroposphere of about 1.7–3.4 $\times$ 10^{-4} s^{-1}. The product of absolute vorticity and divergence is approximately 4–10 $\times$ 10^{-8} s^{-2}, which gives about 1 $\times$ 10^{-3} s^{-1} vorticity generation over the 4–5-h period. This indicates a disturbance could have spun up within the downshear cell that was up to 4–5 times stronger than what already existed in the primary cyclone, if the midtropospheric vertical velocity within the downshear cell averaged 1–2 m s^{-1}. Based on the arguments in section 2, this is a physically achievable vertical velocity in a region of strong lightning. These simple calculations suggest that relating the behavior of Tropical Storm Danny to the idealized simulation was not unreasonable.

It cannot be said for certain that downshear vortex

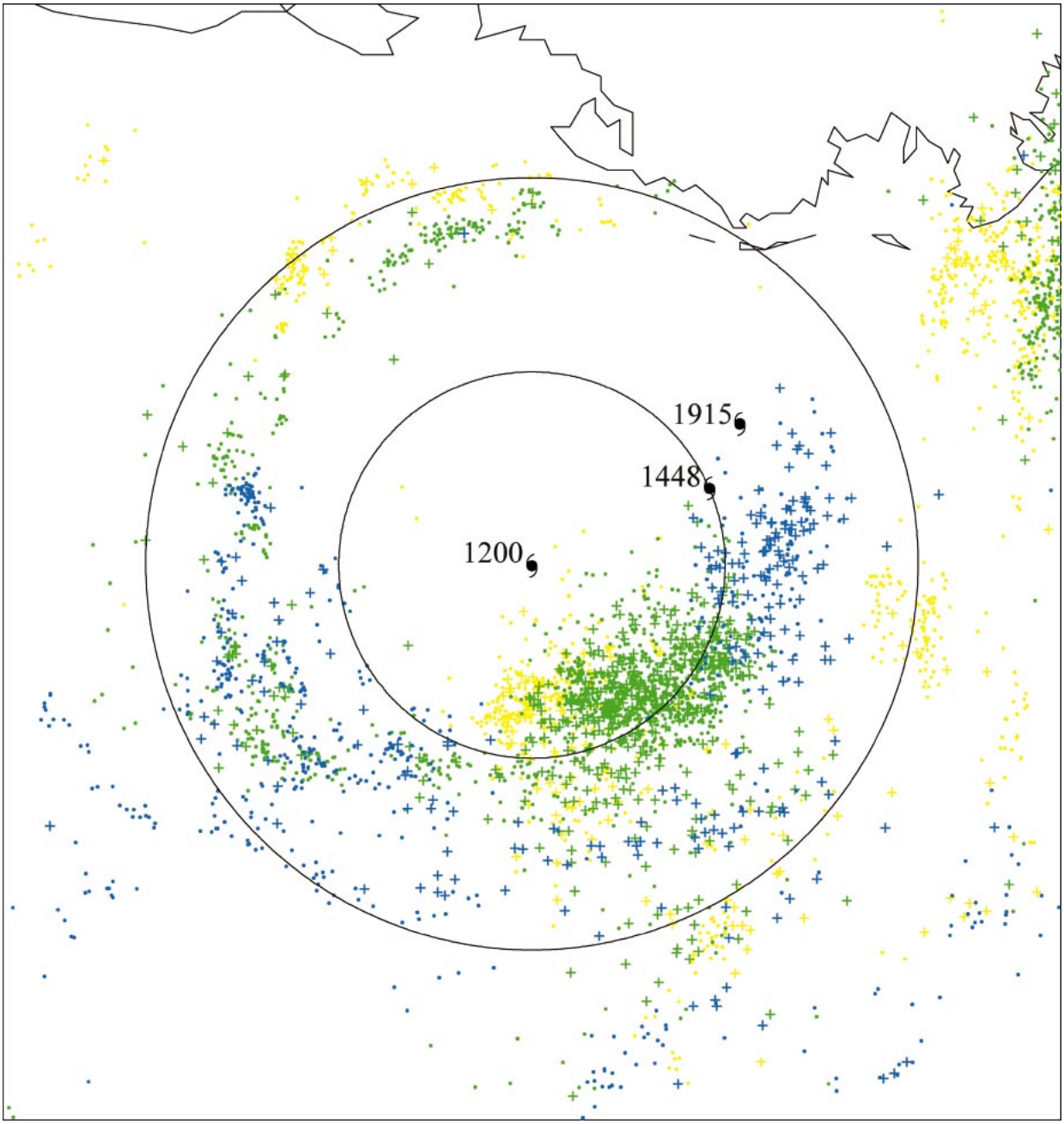

FIG. 10. Evolution of lightning in 2-h increments. Yellow: 0930–1129 UTC 17 Jul; green: 1130–1329 UTC; blue: 1330–1529 UTC. Also shown are the best-track position of the storm at 1200 UTC, the location of the center at 1448 UTC during the first reconnaissance flight after the lightning outbreak, and the location of an eyelike feature at 1915 UTC. The radial rings represent the 50- and 100-km radii at 1200 UTC 17 Jul.

spinup occurred initially at the surface. If cold downdrafts shifted the spinup to higher levels, the final outcome could still be similar. Ritchie and Holland (1997) and Simpson et al. (1997) noted that the interaction of a preexisting surface circulation with one or more midlevel circulations can produce a building down to the surface of the middle-level vorticity and intensification of the surface system. The formal dynamics of this process, including the role of vortex Rossby waves, was presented by Reasor and Montgomery (2001) and Reasor et al. (2004). They described an alignment process among overlapping vortices, the outcome of which was a single nearly upright vortex. It does not appear that the reasoning above depends upon the initial vortex being strongest at the surface. In addition, it is known from reconnaissance aircraft that at 1448 UTC, less than

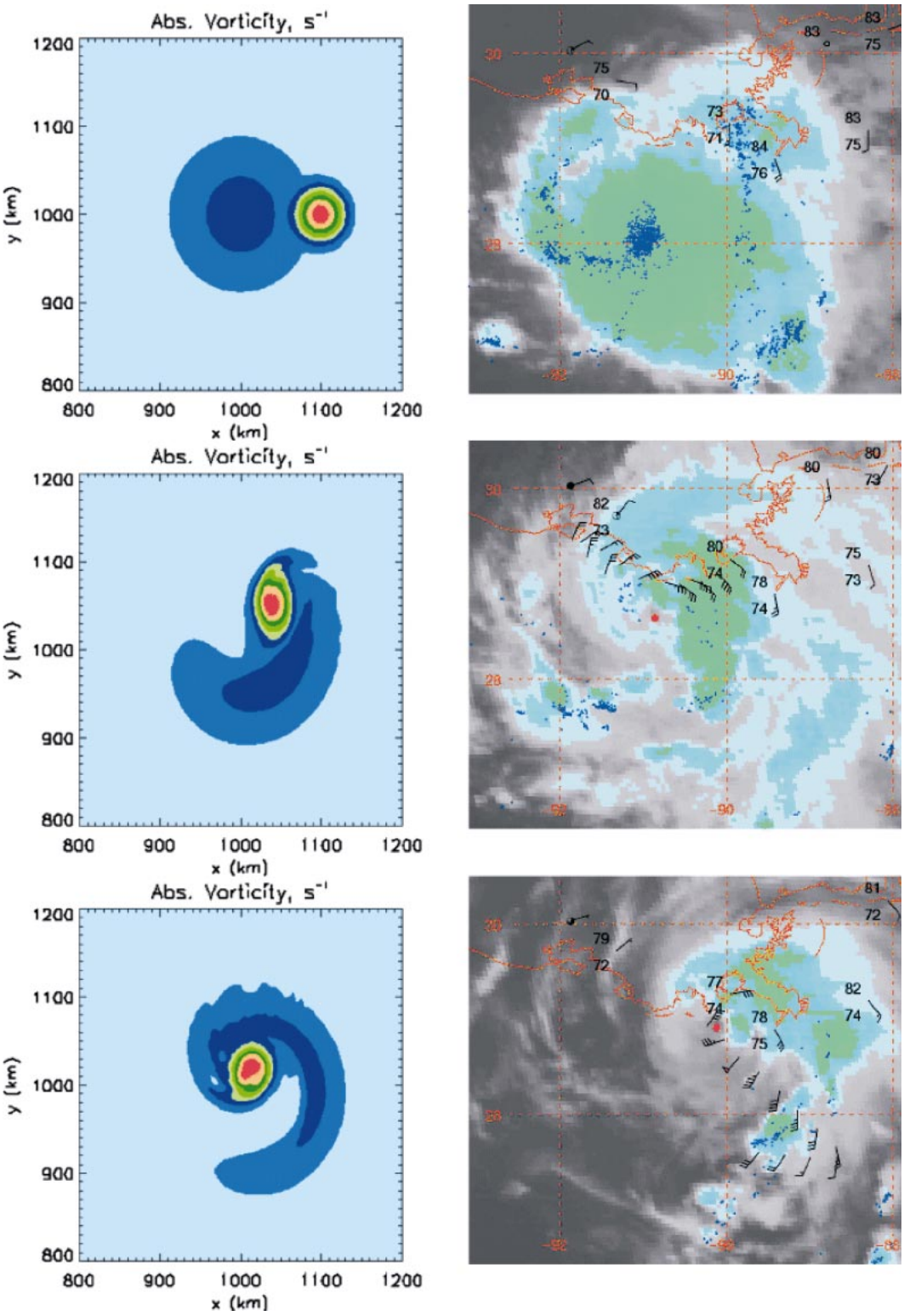

FIG. 11. (left) Vorticity at hours 0, 6, and 12 from the barotropic simulation of two interacting vortices by Enagonio and Montgomery (2001). (right) As in Fig. 7, but for 1300 UTC 17 Jul, 1900 UTC 17 Jul, and 0100 UTC 18 Jul. The filled red circle in the two lower right panels represents the position of an eyelike feature at those times. The small vortex in the top left panel is taken as representative of the spinup occurring within the downshear convective cell in the top right panel, while the large vortex represents the tropical storm circulation to its west seen in Fig. 9.

2 h after the strongest part of convective outbreak, a strong circulation and apparently new center was present at the surface. Finally, the value of θ_e in the oil rig observation to the east of the center at 1200 UTC is 351 K. The midtropospheric minima in θ_e at the same hour in two Louisiana soundings were 336–338 K. The high near-surface θ_e suggests that either cold downdrafts were not occurring, or else significant midlevel moistening had occurred during the previous downshear convection. Either of these allows for the possibility of a lower-tropospheric spinup within the downshear cell.

The arguments above rely on a number of assumptions that cannot be verified, and considerable uncertainty exists in the quantitative estimates of downshear vorticity generation. Nevertheless, the weight of the evidence, based on forecaster comments in real time, track fluctuations, the intensity of the lightning outbreak, and the indirect evidence given in Figs. 9–11, suggests that 1) a strong downshear vortex developed and might have become the primary vortex in the storm, and 2) vortex interactions likely played a critical role in the observed evolution.

b. Evolution of equivalent potential temperature

The U.S. Air Force reconnaissance flights given in Table 1 provided almost continuous coverage of the tropical storm and hurricane after about 1400 UTC 17 July, plus one previous flight during depression stage. Because these flights record temperature and dew points as well as winds, it is possible to compute the distribution of equivalent potential temperature (θ_e). All flight data shown in this paper was collected at elevations between 200 and 500 m and thus give a measure of boundary layer evolution.

Figure 12 shows radial scatterplots of θ_e for four periods: depression stage, early tropical storm stage, late tropical storm stage, and hurricane stage. Values are shown for all azimuths. The center position used to construct Fig. 12 is the best-track value interpolated linearly to 1-min positions. Because the best track is most accurate during reconnaissance flights, and all the panels in Fig. 12 come from reconnaissance flights, the center estimates should be valid. The vertical line in each panel of Fig. 12 shows the mean estimate from reconnaissance of the radius of maximum wind. The horizontal line shows $\theta_e = 355$ K in order to more easily distinguish elevated values.

The storm lies relatively near the coast during the times shown in Fig. 12. Some segments of the flight tracks occurred near land where airflow is moving from land to water. Values of θ_e over land at the surface and at 925 hPa are very similar to those in the outer regions of the tropical cyclone over water at the reconnaissance flight level, which is halfway between those two levels. As a result, the proximity to land should not have a substantial influence on the θ_e distributions in this case.

Figure 12a shows the radial distribution of θ_e during depression stage. Only a slight inward increase of θ_e existed, and the scatter of values was large at all radii. No θ_e maximum existed at the RMW. Figure 12b shows the fields during early tropical storm stage. This is the flight during the time of peak vortex interactions discussed earlier. Although values were elevated from the earlier time, there was once again little evidence of a strong inward increase of θ_e like that known to occur near the RMW of hurricanes (Hawkins and Imbembo 1976). It is argued that high values appeared at all radii owing to the presence of multiple vortices (and thus multiple θ_e maxima) interacting over a wide area.

Figure 12c shows the distribution of θ_e just prior to hurricane intensity, thus at late tropical storm stage. Two significant changes have occurred from the previous plot: values have generally decreased outside the storm core, and many high values appeared within the storm core, just inside of the RMW. This indicates that a radial gradient of θ_e was being established, but a large number of low θ_e values were still present in the core.

Figure 12d shows the θ_e distribution during the first full flight at hurricane intensity on 18 July, beginning just 5 h after the last observation in Fig. 12c. Dramatic changes occurred: low values of θ_e were virtually eliminated from the inner core, and high values of $\theta_e (>355$ K) no longer appeared outside of the 30-km radius. There is no reason to believe that sensor wetting would cease to be a problem at hurricane stage, and thus the lack of inner-core low values of θ_e likely represents a real physical effect. It is hypothesized that both the virtual elimination of low θ_e in the core and the sharp reduction in θ_e variance near the core during hurricane stage reflect the eradication of cold downdrafts in the vicinity of the eyewall. The reduction in θ_e outside the core late on 17 July and early on 18 July might reflect the axisymmetrization of the storm, which would allow low θ_e air at all azimuths at outer radii to be brought into the boundary layer from above as part of the enhanced radial-vertical circulation.

6. Discussion

a. Role of vertical wind shear in the development of Hurricane Danny

The manner in which the storm intensified was directly associated with the formation of downshear convective cells. The vortex developed slowly on 15 and 16 July despite highly asymmetric convection. The mechanisms of Montgomery and Enagonio (1998), in which vortex Rossby waves redistribute convectively generated asymmetric vorticity to the mean vortex, are likely to be relevant during this stage. The development of a tropical storm after the first downshear convective outbreak at 0400–0500 UTC 17 July seemed to continue the process, much like the vortex intensification shown by Möller and Montgomery (2000) in the presence of repeated pulses of downshear convective vorticity sources. The most intense downshear cell, however, ap-

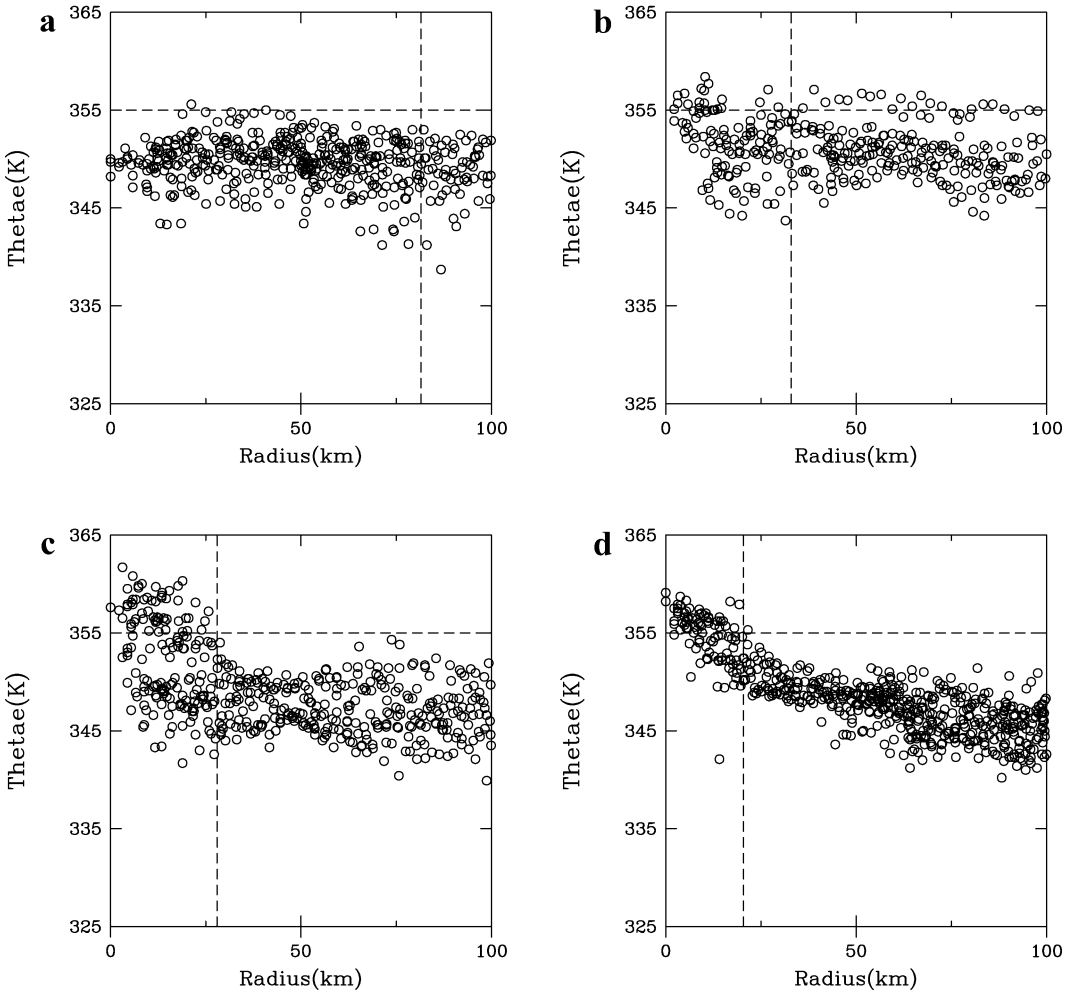

FIG. 12. Radial scatterplots of equivalent potential temperature θ_e(K) calculated from U.S. Air Force reconnaissance flight data with 30-s time resolution. All values are from elevations between 200 and 500 m: (a) 1600–2300 UTC 16 Jul, during depression stage; (b) 1400–2000 UTC 17 Jul, during early tropical storm stage when there were multiple vortex interactions; (c) 2200 UTC 17 Jul–0600 UTC 18 Jul, during late tropical storm stage; and (d) 1100–2100 UTC 18 Jul, the first full flight at hurricane intensity. The vertical dashed line indicates the radius of maximum wind taken from an average of four–six estimates during each flight by reconnaissance aircraft. The value in (c) is averaged from the flights on either side. The horizontal dashed line lies at $\theta_e = 355$ K.

parently was associated with the development of a new center by 1500 UTC 17 July. Thereafter, downshear convective outbreaks did not occur, and the storm intensified to a hurricane in the relative absence of lightning by 0600 UTC 18 July.

On the basis of idealized simulations of circumstances like those in Hurricane Danny, Reasor and Montgomery (2001) argued that if downshear convergence and enhanced convection were larger than could be produced by symmetric mechanisms alone, intensification of a storm could be accelerated by the presence of vertical wind shear. By this reasoning, vertical wind shear might not be an unambiguously negative factor during tropical cyclone genesis. The observations presented in this paper support that view. Strong shear (perhaps greater than 10–15 m s^{-1} over the depth of the troposphere) might prevent genesis, as was shown by Davis and Bosart (2003). But moderate vertical wind shear like the 5–10 m s^{-1} occurring in Danny might contribute to rather than hinder subsequent development. This is supported by the results of Bracken and Bosart (2000), who found that western Atlantic tropical depressions formed in environments with a composite vertical wind shear of 10 m s^{-1}. Broadly speaking, vertical wind shear acts to create additional cyclonic vorticity downshear; the primary vortex (or a more intense downshear vortex) grows by absorption of the vorticity of other convectively generated vortices in the vicinity.

The thermodynamic details of the above process are not certain. Bister and Emanuel (1997) and Raymond

et al. (1998) have argued that midlevel moistening and stabilization must occur before hurricanes can develop, otherwise cold downdrafts interrupt the intensification process. In the presence of vertical wind shear, persistent downshear convection could moisten the column over time, thus reducing downdraft intensity and potentially allowing stronger downshear cells to develop. Figures 4 and 6 in this paper showed that each downshear cell was stronger than the previous one. The final cell occurred near a surface θ_e of 351 K, a value high enough to indicate that substantial cold downdrafts were unlikely. Owing to the lack of data in the vertical in this study, the exact role of midlevel moistening in the growth of Hurricane Danny remains unclear.

b. A speculative conceptual view of the intensification of Hurricane Danny

The wind-induced surface heat exchange (WISHE) theory of Emanuel (1986) and Rotunno and Emanuel (1987) has continued to be refined (e.g., Emanuel 1989, 1997). The essence of the theory has remained the same, however: the prehurricane vortex must be of finite amplitude to develop, axisymmetry and slantwise neutrality are assumed, and development occurs basically as a feedback between surface wind speed and speed-dependent surface moist entropy flux. The WISHE-based developing hurricane contains no cold downdrafts nor strongly buoyant updrafts, and no asymmetric convection.

Smith (2003) showed results from an axisymmetric hurricane boundary layer model in which convective downdrafts were not present. The structure of the model makes it suitable for evaluating the WISHE hypothesis. On the basis of the evolution of winds, surface entropy flux, and equivalent potential temperature, Smith (2003) argued that his model results support the WISHE hypothesis. Smith found a distinct radial variation of θ_e: a slow inward increase well outside the core, an increasingly rapid nonlinear increase approaching the radius of maximum winds, and a continued inward increase inside of the radius of maximum winds. Smith's profile will be used to evaluate when the WISHE process might have occurred in Hurricane Danny.

On 16 July, during tropical depression stage, the evidence from Fig. 12a suggests that no WISHE-like process was occurring; rather, θ_e was nearly constant with radius. It was argued that on 17 July an intense downshear cell created a second circulation center, and the interaction of this with the original vortex initially created a complex disorganized mix of high vorticity and high θ_e over a broad region. Figure 12b shows that θ_e was elevated from the previous period at all radii, but no WISHE signature was present. In this ''pre-WISHE'' stage, little direct coupling could have existed between convection and ocean fluxes as postulated in WISHE: vertical shear exceeded 5 m s^{-1}, the storm was highly asymmetric, interacting vortices were present, and transient highly buoyant convection occurred.

In contrast, Fig. 12c shows that a WISHE-like profile was beginning to develop late on 17 July and early on 18 July, 12–18 h after the vortex interactions began. Figure 12d shows that when hurricane intensity was reached, a dramatic difference in θ_e distribution occurred: low values almost vanished from the storm core, and high values almost vanished from outside the storm core. The result was a monotonic, and increasingly rapid, inward increase of θ_e with radius, remarkably similar to that attributed to the WISHE process by Smith (2003).

It is hypothesized that in Danny, the pre-WISHE stage evolved to a state that the WISHE instability could act by two processes: 1) competition among vortices produced a single near-axisymmetric vortex on the ocean surface, and 2) vertical mixing of moist entropy by convection moistened midlevels and created a nearly slantwise neutral sounding. Evidence for these circumstances in Danny were seen by the development of one dominant vortex and the sharp drop in lightning frequency late on 17 July. By this reasoning, the disturbance then met the requirements of the known finite-amplitude WISHE instability, and development to hurricane intensity followed. Davis and Bosart (2001), in their simulation of the formation of Hurricane Diana (1984), described a similar process. Initially the axisymmetrization of multiple, convectively generated vorticity maxima created a single dominant vortex, and after a 10–12-h period of lower-tropospheric moistening, a WISHE-like intensification produced a hurricane.

The above mechanisms are difficult to observe in real time, because the interaction of vortices occurs on small space and time scales, and the neutralization of a sounding can be inferred only indirectly with available observations. A great deal more work is needed to achieve accurate prediction of the timing of hurricane development from depressions and storms.

Acknowledgments. We are indebted to Mark Powell and Jason Dunion, both from the Hurricane Research Division of NOAA (HRD), for providing us with gridded wind fields used in Fig. 7 from the H*Wind operational surface analyses described by Powell et al. (1998). We also appreciate the efforts of Michael Montgomery of Colorado State University to provide hourly images from the simulations presented by Enagonio and Montgomery (2001). The U.S. Air Force reconnaissance data were retrieved from the archive maintained by John Knaff at the Cooperative Institute for Research in the Atmosphere (CIRA); we appreciate his work in maintaining the archive. Processed lightning data were provided by Vaisala, Inc. Analyses from the European Centre for Medium Range Weather Forecasts were obtained from the National Center for Atmospheric Research (NCAR), which is supported by the National Science Foundation.

We appreciate the substantive comments of Chris Davis from NCAR and an anonymous reviewer. This work was supported by NASA Grant NAG511008 in asso-

ciation with the CAMEX-4 field experiment, and by National Science Foundation Grants ATM-0000673 and ATM-0201752.

REFERENCES

Baker, M. B., A. M. Blyth, H. J. Christian, J. Latham, K. Miller, and A. M. Gadian, 1999: Relationships between lightning activity and various thundercloud parameters: Satellite and modeling studies. *Atmos. Res.,* **51,** 221–236.

Bister, M., and K. A. Emanuel, 1997: The genesis of Hurricane Guillermo: TEXMEX analyses and a modeling study. *Mon. Wea. Rev.,* **125,** 2662–2682.

Black, M. L., R. W. Burpee, and F. D. Marks Jr., 1996: Vertical motion characteristics of tropical cyclones determined with airborne Doppler radar velocities. *J. Atmos. Sci.,* **53,** 802–822.

Black, R. A., and J. Hallett, 1999: The electrification of the hurricane. *J. Atmos. Sci.,* **56,** 2004–2028.

Blackwell, K. G., 2000: The evolution of Hurricane Danny (1997) at landfall: Doppler-observed eyewall replacement, vortex contraction/intensification, and low-level wind maxima. *Mon. Wea. Rev.,* **128,** 4002–4016.

Bolton, D., 1980: The computation of equivalent potential temperature. *Mon. Wea. Rev.,* **108,** 1046–1053.

Bosart, L. F., and J. A. Bartlo, 1991: Tropical storm formation in a baroclinic environment. *Mon. Wea. Rev.,* **119,** 1979–2013.

Bracken, W. E., and L. F. Bosart, 2000: The role of synoptic-scale flow during tropical cyclogenesis over the North Atlantic Ocean. *Mon. Wea. Rev.,* **128,** 353–376.

Brown, R., R. S. Scorer, and P. G. Wickham, 1995: Satellite imagery. *Images in Weather Forecasting: A Practical Guide for Interpreting Satellite and Radar Imagery,* M. J. Bader et al., Cambridge University Press, 7–49.

Cecil, D. L., and E. J. Zipser, 2002: Reflectivity, ice scattering, and lightning characteristics of hurricane eyewalls and rainbands. Part II: Intercomparison of observations. *Mon. Wea. Rev.,* **130,** 785–801.

Corbosiero, K. L., and J. Molinari, 2002: The effects of vertical wind shear on the distribution of convection in tropical cyclones. *Mon. Wea. Rev.,* **130,** 2110–2123.

——, and ——, 2003: The relationship between storm motion, vertical wind shear, and convective asymmetries in tropical cyclones. *J. Atmos. Sci.,* **60,** 366–376.

Cummins, K. L., E. A. Bardo, W. L. Hiscox, R. B. Pyle, and A. E. Pifer, 1995: NLDN'95: A combined TOA/MDF technology upgrade of the U.S. National Lightning Detection Network. *Proc. Int. Aerospace and Ground Conf. on Lightning and Static Electricity,* Williamsburg, VA, U.S. Navy Rep. NAWCADPAX-95-306-PRO, 1–15.

Davis, C. A., and L. F. Bosart, 2001: Numerical simulations of the genesis of Hurricane Diana (1984). Part I: Control simulation. *Mon. Wea. Rev.,* **129,** 1859–1881.

——, and ——, 2003: Baroclinically induced tropical cyclogenesis. *Mon. Wea. Rev.,* **131,** 2730–2747.

DeMaria, M., 1996: The effect of vertical shear on tropical cyclone intensity change. *J. Atmos. Sci.,* **53,** 2076–2087.

——, J.-J. Baik, and J. Kaplan, 1993: Upper-level eddy angular momentum fluxes and tropical cyclone intensity change. *J. Atmos. Sci.,* **50,** 1133–1147.

Eastin, M. D., P. G. Black, and W. M. Gray, 2002: Flight-level thermodynamic instrument wetting errors in hurricanes. Part I: Observations. *Mon. Wea. Rev.,* **130,** 825–841.

Emanuel, K. A., 1986: An air–sea interaction theory for tropical cyclones. Part I: Steady-state maintenance. *J. Atmos. Sci.,* **43,** 585–604.

——, 1989: The finite-amplitude nature of tropical cyclogenesis. *J. Atmos. Sci.,* **46,** 3431–3456.

——, 1997: Some aspects of inner-core dynamics and energetics. *J. Atmos. Sci.,* **54,** 1014–1026.

Enagonio, J., and M. T. Montgomery, 2001: Tropical cyclogenesis via convectively forced vortex Rossby waves in a shallow water primitive equation model. *J. Atmos. Sci.,* **58,** 685–705.

Frank, W. M., and E. A. Ritchie, 2001: Effects of vertical wind shear on the intensity and structure of numerically simulated hurricanes. *Mon. Wea. Rev.,* **129,** 2249–2269.

Hanley, D., J. Molinari, and D. Keyser, 2001: A composite study of the interactions between tropical cyclones and upper-tropospheric troughs. *Mon. Wea. Rev.,* **129,** 2570–2584.

Hawkins, H. F., and S. M. Imbembo, 1976: The structure of a small, intense hurricane: Inez, 1966. *Mon. Wea. Rev.,* **104,** 418–442.

Idone, V. P., D. A. Davis, P. K. Moore, Y. Wang, R. W. Henderson, M. Ries, and P. F. Jamason, 1998a: Performance evaluation of the National Lightning Detection Network in eastern New York, 1, Detection efficiency. *J. Geophys. Res.,* **103,** 9045–9055.

——, ——, ——, ——, ——, ——, and ——, 1998b: Performance evaluation of the National Lightning Detection Network in eastern New York, 2, Location accuracy. *J. Geophys. Res.,* **103,** 9057–9069.

Kossin, J. P., and W. H. Schubert, 2004: Mesovortices in Hurricane Isabel (2003). *Bull. Amer. Meteor. Soc.,* **85,** 9–11.

MacGorman, D. R., and W. D. Rust, 1998: *The Electrical Nature of Storms.* Oxford University Press, 422 pp.

Marks, F. D., Jr., and R. A. Houze Jr., 1987: Inner core structure of Hurricane Alicia from airborne Doppler radar observations. *J. Atmos. Sci.,* **44,** 1296–1317.

Molinari, J., and D. Vollaro, 1989: External influences on hurricane intensity. Part I: Outflow layer eddy angular momentum fluxes. *J. Atmos. Sci.,* **46,** 1093–1105.

——, P. K. Moore, V. P. Idone, R. W. Henderson, and A. B. Saljoughy, 1994: Cloud-to-ground lightning in Hurricane Andrew. *J. Geophys. Res.,* **99,** 16 665–16 676.

——, S. Skubis, and D. Vollaro, 1995: External influences on hurricane intensity. Part III: Potential vorticity structure. *J. Atmos. Sci.,* **52,** 3593–3606.

——, P. Moore, and V. Idone, 1999: Convective structure of hurricanes as revealed by lightning locations. *Mon. Wea. Rev.,* **127,** 520–534.

Möller, J. D., and M. T. Montgomery, 2000: Tropical cyclone evolution via potential vorticity anomalies in a three-dimensional balance model. *J. Atmos. Sci.,* **57,** 3366–3387.

Montgomery, M. T., and B. F. Farrell, 1993: Tropical cyclone formation. *J. Atmos. Sci.,* **50,** 285–310.

——, and J. Enagonio, 1998: Tropical cyclogenesis via convectively forced vortex Rossby waves in a three-dimensional quasigeostrophic model. *J. Atmos. Sci.,* **55,** 3176–3207.

Orville, R. E., 1991: Calibration of a magnetic direction finding network using measured triggered lightning return stroke peak currents. *J. Geophys. Res.,* **96,** 17 135–17 142.

Pasch, R. J., 1998: Preliminary report: Hurricane Danny 16–26 July 1997. National Hurricane Center Rep., 18 pp. [Available online at http://www.nhc.noaa.gov/1997danny.html.]

Powell, M. D., S. H. Houston, L. R. Amat, and N. Morissaeu-Leroy, 1998: The HRD real-time hurricane wind analysis system. *J. Wind Eng. Ind. Aerodyn.,* **77–78,** 53–64.

Raymond, D. L., C. Lopez-Carrillo, and L. Lopez Cavazos, 1998: Case-studies of developing east Pacific easterly waves. *Quart. J. Roy. Meteor. Soc.,* **124,** 2005–2034.

Reasor, P. D., and M. T. Montgomery, 2001: Three-dimensional alignment and corotation of weak, TC-like vortices via linear vortex Rossby waves. *J. Atmos. Sci.,* **58,** 2306–2330.

——, ——, and L. D. Grasso, 2004: A new look at the problem of tropical cyclones in vertical shear flow: Vortex resiliency. *J. Atmos. Sci.,* **61,** 3–22.

Ritchie, E. R., and G. J. Holland, 1997: Scale interactions during the formation of Typhoon Irving. *Mon. Wea. Rev.,* **125,** 1377–1396.

Rotunno, R., and K. A. Emanuel, 1987: An air–sea interaction theory for tropical cyclones. Part II: Evolutionary study using a non-

hydrostatic axisymmetric numerical model. *J. Atmos. Sci.,* **44,** 542–576.

Samsury, C. E., and R. E. Orville, 1994: Cloud-to-ground lightning in tropical cyclones: A study of Hurricanes Hugo (1989) and Jerry (1989). *Mon. Wea. Rev.,* **122,** 1887–1896.

Simpson, J., E. Ritchie, G. J. Holland, J. Halverson, and S. Stewart, 1997: Mesoscale interactions in tropical cyclone genesis. *Mon. Wea. Rev.,* **125,** 2643–2661.

Smith, R. K., 2003: A simple model of the hurricane boundary layer. *Quart. J. Roy. Meteor. Soc.,* **129,** 1007–1028.

Sutcliffe, R. C., 1947: A contribution to the problem of development. *Quart. J. Roy. Meteor. Soc.,* **73,** 370–383.

Zipser, E. J., and K. R. Lutz, 1994: The vertical profile of radar reflectivity of convective cells: A strong indicator of storm intensity and lightning probability? *Mon. Wea. Rev.,* **122,** 1751–1759.